Theoretical Study of the Dynamics of Ar Collisions with C_2H_6 and C_2F_6 at Hyperthermal Energy

Uroš Tasić, Pyae Hein, and Diego Troya*

Department of Chemistry, Virginia Tech, 107 Davidson Hall, Blacksburg, Virginia 24061-0212

Received: February 14, 2007; In Final Form: March 6, 2007

We present a classical-trajectory study of the dynamics of high-energy (5−12 eV) collisions between Ar atoms and the C_2H_6 and C_2F_6 molecules. We have constructed the potential-energy surfaces for these systems considering separately the Ar−molecule interactions (intermolecular potential) and the interactions within the molecule (intramolecular potential). The intermolecular surfaces consist of pairwise empirical potentials derived from high-accuracy ab initio calculations. The intramolecular potentials for C_2H_6 and C_2F_6 are described using specific-reaction-parameters semiempirical Hamiltonians and are calculated "on the fly", i.e., while the trajectories are evolving. Trajectory analysis shows that C_2F_6 absorbs more energy than C_2H_6 and is more susceptible to collision-induced dissociation (CID). C−C bond-breakage processes are more important than C−H or C−F bond breakage at the energies explored in this work. Analysis of the reaction mechanism for CID processes indicates that, although C−C breakage is mostly produced by side-on collisions, head-on collisions are more efficient in producing C−F or C−H dissociation. Our results suggest that high-energy collisions between closed-shell species of the natural low-Earth-orbit environment and spacecraft can contribute to the observed degradation of polymers that coat spacecraft surfaces.

Introduction

A major impediment in the development of theoretical studies of the dynamics of multidimensional chemical reactions is the lack of a clear strategy to obtain accurate analytic potential-energy surfaces (PES) describing the forces acting on the nuclei in their passage from reagents to products. Direct-dynamics calculations are an alternative to constructing analytic PES based on obtaining the forces acting on the nuclei directly from electronic-structure calculations whenever needed in the dynamics calculations.[1] A problem with direct dynamics is that the large number of force calculations required in reaction-dynamics studies (in the 10^6-10^8 range in routine studies) significantly constrains the type and quality of electronic-structure methods that can be used with this approach. For instance, ab initio methods, including Hartree−Fock (HF), or density-functional theory (DFT) methods, pose a prohibitive computational overhead when used in extensive direct-dynamics studies of chemical reactions that contain more than a handful of heavy atoms.

Semiempirical Hamiltonians are an attractive alternative to ab initio or DFT in direct-dynamics calculations, because their computational cost is substantially smaller than that of any first-principles method.[2] The enormous decrease in the computational expenditure of semiempirical Hamiltonians is mainly due to the neglect and parametrization of expensive electronic integrals, and the use of minimal basis sets. Unsurprisingly, although these approximations make semiempirical Hamiltonians orders of magnitude faster than first-principles methods for large systems, they often result in sizable inaccuracies.

A simple way to improve the accuracy of a semiempirical Hamiltonian for a specific reaction is to modify the original parameters so that the Hamiltonian better reproduces experimental or higher-level theoretical information only for that reaction. Truhlar and co-workers pioneered the development of specific-reaction-parameter (SRP) semiempirical Hamiltonians for statistical calculations of thermal rate constants and kinetic isotope effects.[3] Later, Hase developed SRP Hamiltonians for $O(^3P)$ + alkane reactions and used them to perform chemical-dynamics simulations.[4,5] More recently, our group has been interested in exploring the adequacy of SRP Hamiltonians for reaction-dynamics studies of small gas-phase reactions. In particular, we have developed SRP semiempirical Hamiltonians for the $X + CH_4 \rightarrow HX + CH_3$ (where $X = O(^3P)$,[6] F,[7] and Cl[8]) reactions. Results of quasi-classical-trajectory calculations that apply these SRP Hamiltonians provided product-state distributions in quantitative agreement with experiments, improving over earlier theoretical data. These results suggest that careful development of SRP Hamiltonians is a promising technique to obtain predictive PES for reaction-dynamics studies.

In this work, we derive SRP Hamiltonians to treat dissociation of the C_2H_6 and C_2F_6 molecules ensuing impact with Ar atoms at high translational energies. High-energy collisions between closed-shell species and hydrocarbons are relevant to the degradation of polymer materials in low Earth orbit (LEO) (an altitude of 200−700 km). A spacecraft traveling in LEO at ∼7.4 km/s collides with ambient gaseous species (mainly $O(^3P)$, O_2, N_2, and Ar, at low altitudes[9]) at high collision energies (∼4.5, 9.0, 8.0, and 11.3 eV for $O(^3P)$, O_2, N_2, and Ar, respectively). These high-energy collisions are blamed for the observed fast degradation of the polymers that coat spacecraft.[10,11] Molecular studies aimed at understanding the atomic-level details of the polymer degradation processes have mostly considered the interactions of $O(^3P)$, the most abundant species in LEO, with hydrocarbons.[5,12−17] Although these studies have unveiled a wealth of information about the microscopic mechanism of hydrocarbon degradation in LEO, there is an increasing need to understand the effect of ambient species other than

* Author to whom correspondence should be addressed. E-mail address: troya@vt.edu.

10.1021/jp071287q CCC: $37.00
Published on Web 04/13/2007

$O(^3P)$. Minton and co-workers reported that hyperthermal beams of Ar atoms caused the ejection of CO and CO_2 molecules from oxidized polymer surfaces.[18] They also showed that hyperthermal Ar atoms can transfer large amounts of energy to hydrocarbon molecules.[19] This same group has recently given evidence that, although the fluorinated ethylene−propylene copolymer (FEP Teflon) is inert to atomic oxygen at collision energies comparable to those in LEO (~5 eV), it undergoes degradation upon bombardment with Ar atoms at energies of >8 eV.[20]

These experimental efforts suggest that species other than $O(^3P)$ should not be neglected in a complete characterization of polymer degradation in LEO. Our first efforts directed at unveiling the atomic-level details of Ar−hydrocarbon hyperthermal collisions focused on encounters of fast Ar atoms with CH_4 and CF_4 molecules.[21] We showed that, at collision energies (E_{coll}) of >9 eV, large amounts of energy transfer to CF_4 can result in C−F dissociation. In this paper, we intend to advance our understanding of hydrocarbon degradation via collision-induced dissociation by investigating the possibility of C−C bond breakage. A second goal of this paper is to assess the possibility that SRP Hamiltonians can simultaneously describe two reactive channels with accuracy.

This paper is organized as follows: First, we describe development of intermolecular and intramolecular PES for the Ar−C_2H_6 and Ar−C_2F_6 systems from high-quality ab initio calculations. We then present classical-trajectory calculations of Ar + C_2H_6 and Ar + C_2F_6 collisions at hyperthermal energies. Finally, we give a summary and conclusions.

Potential-Energy Surfaces

In this section, we describe the development of the PES that we have used to investigate the dynamics of high-energy Ar + C_2H_6 and Ar + C_2F_6 collisions. We explain, separately, the derivation of the intermolecular and intramolecular terms that compose our PES.

Ar−C_2H_6 and Ar−C_2F_6 Intermolecular Potential-Energy Surfaces. Intermolecular potentials suitable for low-energy collisions between Ar and regular and perfluorinated alkanes have been recently published by Alexander et al.[22] In this work, we follow the strategy adopted in that previous study to extend the Ar−alkane intermolecular potentials to high energies. We note that the intermolecular potentials developed in this work apply ab initio information at a much higher level of theory than in our previous study of Ar + CH_4 and Ar + CF_4 hyperthermal collisions.[21]

We have derived analytic two-body potentials for the Ar−H and Ar−C, and for the Ar−F and Ar−C pairs that are applicable to simulations of hyperthermal Ar + C_2H_6 and Ar + C_2F_6 collisions, respectively. These analytic potentials are based on ab initio calculations of the Ar−CH_4 and Ar−CF_4 PES. Because of the fact that we intend to describe high-energy collisions accurately, we have given special emphasis to the description of repulsive walls by including ab initio points that represent interaction energies of up to 17 eV (400 kcal/mol). We have characterized the intermolecular PES by performing high-level ab initio calculations along three representative approaches of Ar to the molecules: (i) perpendicular to one of the faces of the CX_4 (where X = H, F) tetrahedron (face approach, C_{3v} symmetry), (ii) bisecting an angle X−C−X (edge approach, C_{2v} symmetry), and (iii) collinear to a C−X bond (vertex approach, C_{3v} symmetry). Schematics of these approaches can be found in Figure 1 of ref 21. For Ar−CH_4, we have calculated 40−50 points in each of the approaches from an Ar−C distance of 6.0 Å to distances resulting in ~17 eV repulsions. For Ar−CF_4, we have scanned the Ar−C distance starting at 6−7 Å. In this case, we have calculated 60−70 points per approach. In each of the points, we have used the Gaussian03 program[23] to calculate the Ar−molecule interaction energy at the MP2/aug-cc-pvdz, MP2/aug-cc-pvtz, MP2/aug-cc-pvqz, and CCSD(T)/aug-cc-pvdz levels. We have removed the basis-set superposition error using the standard counterpoise method in every point of the PES calculated. During the PES scans, we have held the CH_4 and CF_4 molecules frozen in their tetrahedral geometries with r(C−H) = 1.089 Å and r(C−F) = 1.330 Å, respectively.

At the MP2 level, we observe that the intermolecular potential decreases as the basis set increases in each point of the PES that we have calculated. This trend replicates our earlier findings at low energies.[22] In that earlier paper, we also reported that CCSD(T)/aug-cc-pvdz intermolecular energies were only slightly higher than MP2/aug-cc-pvdz. This trend is also seen at high energies in this work, with CCSD(T)/aug-cc-pvdz intermolecular energies being ~2% above MP2/aug-cc-pvdz values in all approaches. Given the small differences between MP2 and CCSD(T) intermolecular energies with the aug-cc-pvdz basis set, we have used the focal-point approach of Allen et al.[24] to estimate CCSD(T) energies extrapolated at the complete basis-set limit from MP2 calculations. The focal-point approach emerges from the assumption that the differences between MP2 and CCSD(T) calculations are independent of the basis set. Using this approximation, we apply the minor differences between MP2 and CCSD(T) energies with the aug-cc-pvdz basis set to estimate CCSD(T) energies with the aug-cc-pvtz and aug-cc-pvqz basis sets from MP2 calculations with those basis sets. Hereafter, we refer to CCSD(T) energies estimated using the focal-point approach as fp-CCSD(T).

Using the fp-CCSD(T)/aug-cc-pvtz and aug-cc-pvqz energies, we have applied a two-point formula[25] to obtain a complete basis-set (CBS) estimate of the fp-CCSD(T) energies. We have verified that this two-point extrapolation provides energies well within 1% of those calculated with the popular extrapolation scheme of Peterson et al.[26] for both the Ar−CH_4 and Ar−CF_4 systems at all energies. Figure 1 shows the most-accurate intermolecular potential energies calculated in this work, as a function of the Ar−C distance for both systems. The main figures show the entire energy range explored, and the insets display the long-range attractive well region caused by dispersion interactions. An extensive description of the trends in the well region can be found elsewhere.[22] Briefly, the face approach is the most attractive, followed by edge and vertex for both systems. The wells are slightly deeper (by ~0.15 kcal/mol) for the perfluorinated systems than for the hydrogenated systems, because of an increase in the polarizability of the molecule upon fluorination. Given that the focus of this paper is on collisions that occur at several electron volts, it is likely that these differences in the attractive region of the potential are not important. On the other hand, the repulsive wall likely has a key role in determining the dynamics. The repulsive walls in Ar−CF_4 are shifted to longer Ar−C distances than those in Ar−CH_4, by ~0.15, 0.30, and 0.55 Å for the face, edge, and vertex configurations, respectively. The steepness of the repulsive walls is similar for CH_4 and CF_4 in the face configuration. However, in the edge and vertex configurations, the repulsive walls of Ar−CF_4 are ~10% and ~15% steeper than those of Ar−CH_4.

We have used the fp-CCSD(T)/CBS energies displayed in Figure 1 to obtain pairwise analytic potentials that describe intermolecular interactions in collisions of Ar atoms with C_2H_6 and C_2F_6. The analytic potential of each pair of atoms is based

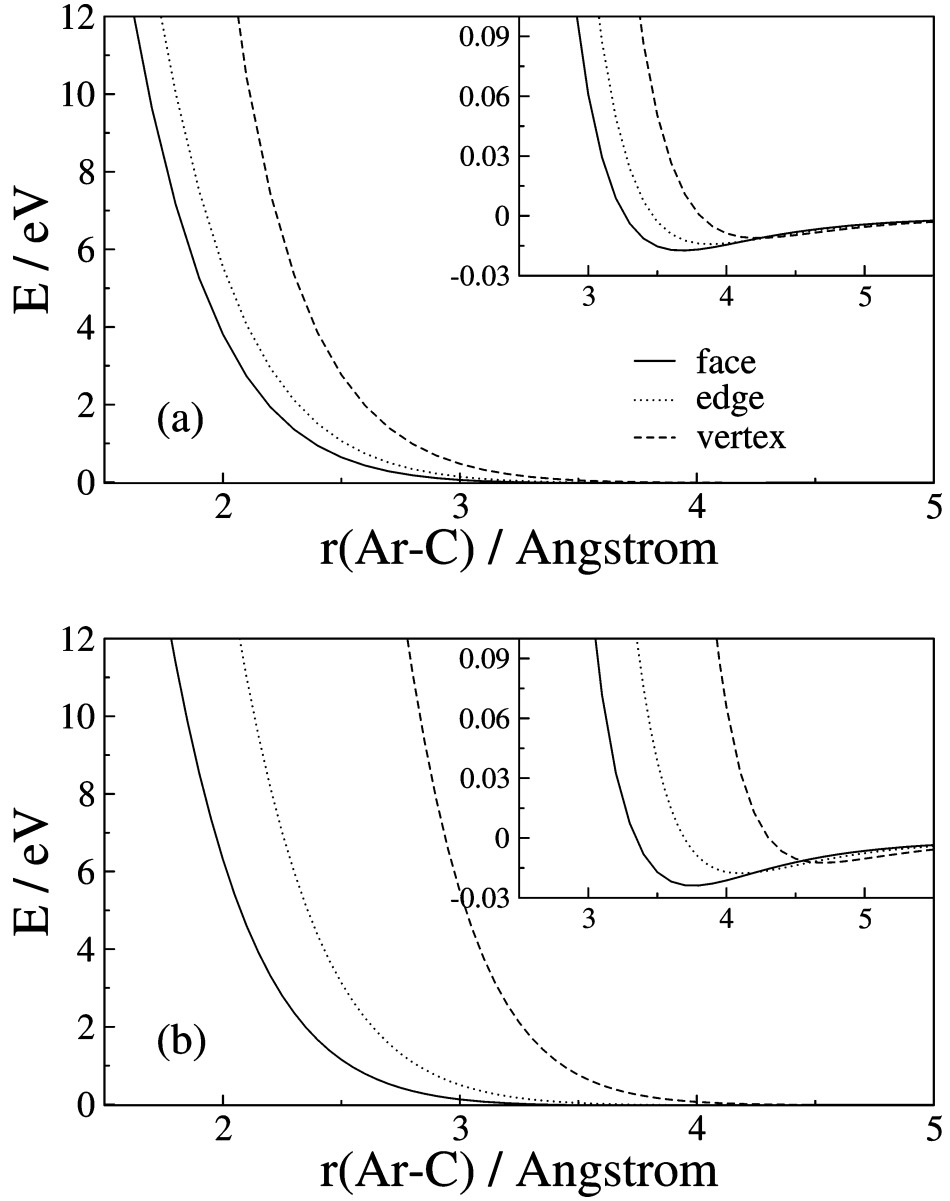

Figure 1. Calculated intermolecular potential-energy surfaces (PES) in approaches of the Ar atom to the (a) CH_4 and (b) CF_4 molecules. The data correspond to fp-CCSD(T)/CBS calculations (see text). Insets show the attractive well region.

on the generalized Buckingham function in eq 1:

$$U = \frac{A}{\exp(Br)} + \frac{C}{r^n} \tag{1}$$

where U and r are the potential energy and distance between the Ar atom and one of the CX_4 atoms, respectively. The total intermolecular potential energy is taken to be the sum of the potential energies of all the pairs of atoms. In each system, there are two types of interactions: Ar−C and Ar−H for Ar−CH_4, and Ar−C and Ar−F for Ar−CF_4. Each interaction is characterized by a set of four parameters: *A*, *B*, *C*, and *n*. The set of eight optimal parameters per system is obtained via nonlinear minimization of the differences between the total Buckingham energy and the fp-CCSD(T)/CBS points for the three approach configurations. The best-fit parameters are given in Table 1, and the best-fit curves and reference ab initio points are shown in Figure 2 for the Ar−CH_4 and Ar−CF_4 systems.

As can be seen in Figure 2, the analytic functions reproduce the ab initio data quite accurately. The deviations are generally small for both systems, but are slightly lower for Ar−CF_4.

TABLE 1: Parameters of the Buckingham Pairwise Potentials Describing Ar−Alkane and Ar−Perfluoroalkane Intermolecular Interactions[a]

atom pair	*A*	*B*	*C*	*n*
		Ar−CH_4		
Ar−C	64 897.193034	3.377437	−911.267281	5.828702
Ar−H	9 862.755560	3.467973	−91.353565	5.370459
		Ar−CF_4		
Ar−C	19 017.011295	3.148883	−397.187335	6.995127
Ar−F	110 093.847032	3.789906	−2 244.052263	6.903518

[a] Units are such that if internuclear distances are given in angstroms, energies are given in units of kcal/mol.

Typical deviations in the attractive region are 0.03 ± 0.02 kcal/mol for Ar−CH_4 and 0.01 ± 0.02 kcal/mol for Ar−CF_4. In the repulsive region, the average deviations are 7% ± 6% for Ar−CH_4 and 5% ± 4% for Ar−CF_4. We note that these deviations between the fit and fp-CCSD(T)/CBS data are much smaller than those that would emerge if we had used a lower level of ab initio theory for the grid of points involved in the fit. For instance, the deviations between the analytical function and fp-

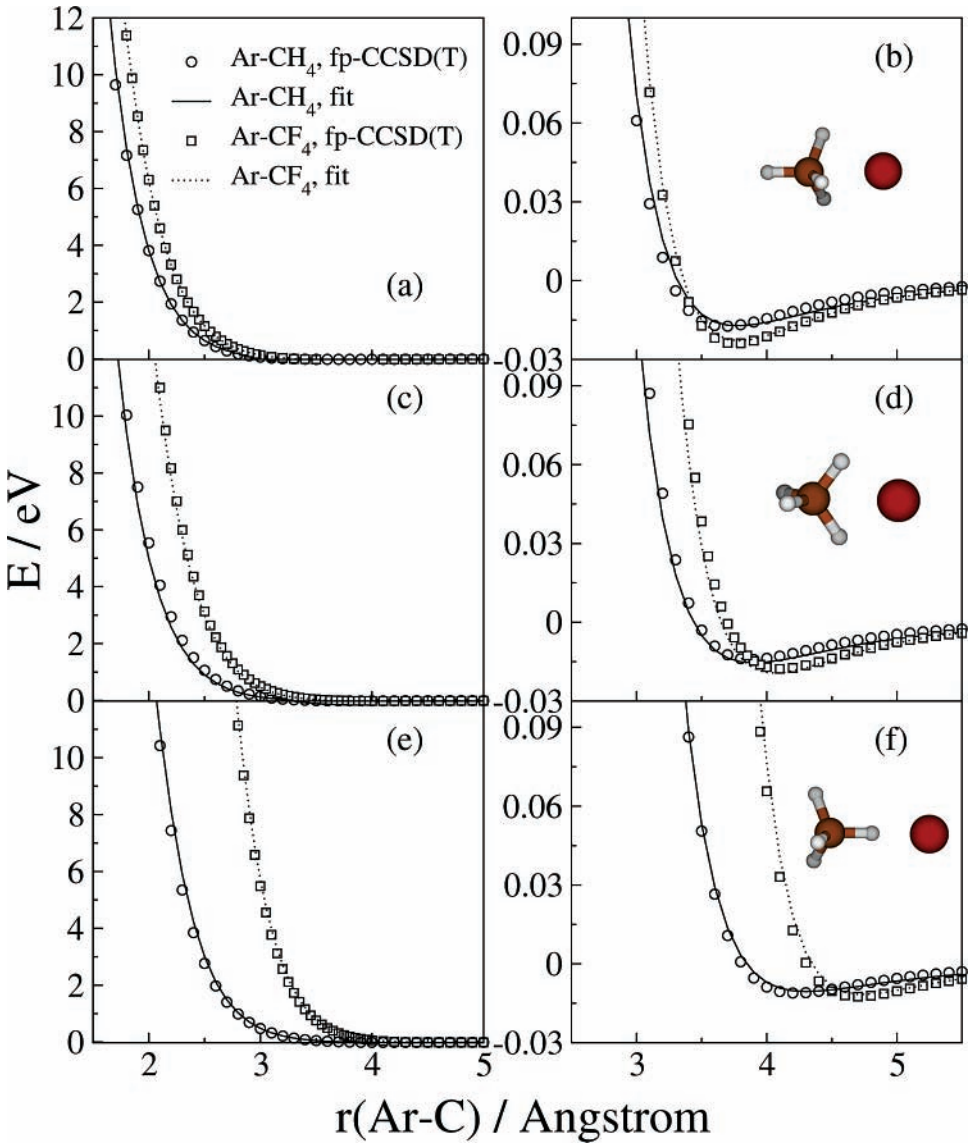

Figure 2. Comparison of fp-CCSD(T)/CBS and analytic intermolecular PES in approaches of the Ar atom to the CH_4 and CF_4 molecules: (a) and (b) show face approaches, (c) and (d) show edge approaches, and (e) and (f) show vertex approaches. Panels (a), (c), and (e) show the repulsive wall, and panels (b), (d), and (f) show the attractive well region.

CCSD(T)/CBS data are approximately a factor of 2 and a factor of 4 smaller than between CCSD(T)/aug-cc-pvdz and fp-CCSD(T)/CBS energies for Ar−CH_4 and Ar−CF_4, respectively.

There are several notes about our fitting procedure worth mentioning. First, we constrained the parameters in the fitting process so that the first term, $A/\exp(Br)$, is repulsive, and the second term, C/r^n, is attractive. These constraints ensure that the analytic potential is well-behaved for nonequilibrium CX_4 configurations and for very small Ar−molecule separations. Second, to gain addition flexibility, we did not enforce the attractive term to possess a traditional inverse sixth-order dependence ($n = 6$) in the fits. Third, the addition of a third term, D/r^m, to the Buckingham function did not lead to significant fit improvements. Finally, we note that the Buckingham potential always has a limited range of applicability, because it turns over at very short distances. Analysis shows that our analytical potentials are adequate for intermolecular energies up to ∼17 and ∼24 eV for Ar−CH_4 and Ar−CF_4, respectively.

The analytic potentials previously discussed have been derived from three selected approaches of the Ar atom to the CX_4 molecules (face, edge, and vertex). Using the Ar−CF_4 system, we now demonstrate that these analytic potentials are able to accurately represent other regions of the surface that were not explicitly included in the fit. Ideally, one would like to compare the analytic potentials in Table 1 with fp-CCSD(T)/CBS data for a large number of points of the Ar−CF_4 PES. However, because of the computational cost of the fp-CCDS(T)/CBS energy evaluations, we have derived an analytic potential based on MP2/aug-cc-pvdz energies for the face, edge, and vertex Ar−CF_4 approaches and compared it with MP2/aug-cc-pvdz energies in other regions of the Ar−CF_4 PES. The fitting procedure of this lower-level potential is analogous to that previously described for fp-CCSD(T)/CBS energies. To generate a random grid of points of the Ar−CF_4 surface, we place Ar atoms randomly on the surface of spheres centered at the C atom with radii in the range of 1.8−5.5 Å. The geometries are selected such that the ab initio energies do not exceed 17 eV (∼400 kcal/mol), which is the limit in our fits. Overall, we generated 706 points with this procedure. The agreement between the analytic and ab initio energies in this set of configurations that were not included in the fit is generally good. The average relative error is 4.6% ± 2.8% in the region of the repulsive wall, and the average absolute error is 0.03 ±

0.05 kcal/mol in the region of the attractive well. These deviations match those of the points for the face, edge, and vertex approaches that were explicitly included in the fit. One can thereby conclude from this test that the analytic pairwise potentials for $Ar-CH_4$ and $Ar-CF_4$ derived from fp-CCSD-(T)/CBS energies along the face, edge, and vertex approaches only, accurately represent the entire PES.

We now address the extensibility of the pairwise potentials derived from $Ar-CX_4$ calculations to $Ar-C_2X_6$. We have calculated several points along six approaches of the Ar atom to the C_2F_6 molecule at the MP2/aug-cc-pvdz level, and we have compared them with the analytical potential based on points calculated at this level for $Ar-CF_4$. The six approaches of the Ar atom to C_2F_6 studied ab initio are the perpendicular of the Ar atom to the C−C bond in C_2F_6, collinear to a C−F bond with 0° and 180° Ar−F−C−C dihedrals, and bisecting the F−C−C and F−C−F angles and collinear to the C−C bond. We have calculated 26 ab initio points in each approach from the asymptote to energies up to ∼17 eV. We find that the average error of our analytic potentials is 0.02 kcal/mol in the attractive well, and 4% in the repulsive wall. This implies that pairwise potentials derived from $Ar-CX_4$ are accurate to treat $Ar-C_2X_6$.

Finally, we have investigated the performance of our Ar−alkane analytic potentials for situations in which the molecules are not in their equilibrium configuration. This test is important because the focus of this paper is on alkane collision-induced dissociation, whereby C_2H_6 and C_2F_6 experience large distorsions while the Ar atom is close to the molecules. We have performed MP2/aug-cc-pvdz calculations for six approaches of the Ar atom to a distorted CF_4 molecule in which one of the C−F bonds is 2.2 Å long. The distorted CF_4 forms a triangular prism (C_{3v} symmetry) and the six approaches are collinear to the two dissimilar C−F bonds, bisecting the two dissimilar F−C−F angles, and perpendicular to the two dissimilar faces of the prism. We have calculated 26 ab initio points in each approach from the asymptote to energies up to ∼17 eV. The average error in the well region is 0.07 kcal/mol and 10% in the repulsive wall. Analogously, we have calculated the intermolecular energy of the six Ar atom approaches to the C_2F_6 molecule previously mentioned, but with an elongated C−C bond (2.5 Å), or an elongated C−F bond (2.3 Å). In this case, we have calculated 27 ab initio points from the asymptote to energies up to ∼17 eV in each approach to each of the distorted molecules (324 total points). The error in the well regions is ∼0.05 kcal/mol and ∼8% in the repulsive wall for these approaches to distorted C_2F_6 molecules. We note that, in actual collisions, the Ar atom recoils very fast from the molecule. Therefore, by the time the breaking bond becomes longer than the distances previously explored, the Ar atom is typically no longer interacting with the breaking molecule. Thus, we have not studied the accuracy of the intermolecular potentials in situations where the Ar atom is interacting with a molecule with a bond longer than 2.5 Å.

We conclude that the analytic potential built from three selected approaches of the Ar atom to the CF_4 molecule in its equilibrium configuration is able to describe accurately not only the intermolecular potential of the Ar atom approaching the C_2F_6 molecule in equilibrium, but also in distorted conformations, such as those encountered in collision-induced dissociation processes.

C_2H_6 and C_2F_6 Intramolecular Potential-Energy Surfaces. In this section, we describe the development of SRP Hamiltonians for the C_2H_6 and C_2F_6 molecules, which we have used to evaluate the intramolecular potential energy and energy gradients in the trajectory simulations described in the next section.

Collisions of hyperthermal Ar atoms with C_2H_6 and C_2F_6 molecules can produce dissociation in these molecules if the energy transferred to a bond stretch is in excess of the bond dissociation energy (BDE). Table 2 shows the C−C and C−H BDEs in C_2H_6 as predicted by various electronic-structure methods, in comparison with experiments.[27−30] The popular PM3[31] and AM1[32] semiempirical Hamiltonians underestimate the experimental C−C and C−H BDEs by as much as 1 eV. Therefore, reaction-dynamics calculations using these semiempirical Hamiltonians will likely underestimate the threshold for collision-induced dissociation in hyperthermal Ar + C_2H_6 encounters. The reaction energies provided by the MSINDO[33] semiempirical Hamiltonian are notably closer to the first-principles estimates and experiment. DFT B3LYP calculations with the aug-cc-pvdz and aug-cc-pvtz correlation-consistent basis sets slightly underestimate both the C−C and C−H BDEs. The dependence of the B3LYP results on the basis set seems minor, with differences between aug-cc-pvdz and aug-cc-pvtz results being ∼0.05 eV (roughly, 1 kcal/mol). MP2 calculations with the same basis sets compare well with B3LYP for the C−H dissociation, but are noticeably more similar to experiments for the C−C dissociation.

The relatively low number of electrons in the C_2H_6 molecule enables calculation of reaction energies using coupled-cluster theory with single, double, and perturbative triple excitations in combination with an augmented double-ζ basis set (CCSD(T)/aug-cc-pvdz). These calculations underestimate the experimental dissociation energies of both the C−H and C−C bonds by ∼0.25 eV. To learn if this difference with experiment is due to a basis set that is too small, we have conducted single-point CCSD(T) calculations with larger basis sets using geometries calculated at lower levels of theory. The demonstration that these dual-level calculations are accurate is given by comparison of the CCSD(T)/aug-cc-pvdz dissociation energies with CCSD(T)/aug-cc-pvdz single-point calculations employing geometries and harmonic frequencies calculated at the B3LYP/aug-cc-pvdz, MP2/aug-cc-pvdz, and MP2/aug-cc-pvtz levels. The dual-level calculations are in excellent agreement with the "pure" CCSD(T)/aug-cc-pvdz calculation, giving evidence that dual-level calculations are appropriate in this case.

CCSD(T)/aug-cc-pvtz calculations predict dissociation energies much more similar to the experiment than CCSD(T)/aug-cc-pvdz calculations. The gap between CCSD(T) calculations and experiments is diminished further when using the aug-cc-pvqz basis set, indicating that the difference between CCSD-(T)/aug-cc-pvdz energies and experiments previously noted is, indeed, a basis-set effect. Extrapolation of the CCSD(T) energies to the complete basis-set limit (CCSD(T)/CBS) using a two-point formula[25] provides BDEs in good agreement with experiments, as expected. Remarkably, the popular complete-basis set models G2MP2 and CBS-Q accurately reproduce CCSD(T)/CBS results, despite requiring much less computer time.

Figures 3a and 3b respectively show the C−H and C−C minimum-energy dissociation curves at various levels of electronic-structure theory. The curves correspond to relaxed scans of the C−H and C−C coordinates and have been calculated using an unrestricted reference and an initial orbital guess in which the HOMO and LUMO are mixed to generate inequivalent α and β orbital spaces. Dutta and Sherrill indicated that CCSD(T) was the single-reference method which provided results in closest agreement to FULL-CI calculations for C−H bond dissociation in CH_4.[34] Because FULL-CI calculations for

TABLE 2: Experimental and Calculated C_2H_6 Bond Dissociation Energies[a]

	bond dissociation energy, BDE (eV)			
	C_2H_5-H		CH_3-CH_3	
	with ZPE	classical (without ZPE)	with ZPE	classical (without ZPE)
PM3	3.261	3.676	2.794	3.212
AM1	3.296	3.686	2.974	3.353
MSINDO	3.835	4.230	3.472	3.867
B3LYP/adz	4.149	4.562	3.610	4.010
B3LYP/atz	4.191	4.607	3.564	3.970
MP2/adz	4.106	4.518	3.806	4.207
MP2/atz	4.253	4.669	3.907	4.319
CCSD(T)/adz	4.137	4.548	3.638	4.042
CCSD(T)/adz//B3LYP/adz	4.137	4.550	3.641	4.041
CCSD(T)/atz//B3LYP/adz	4.272	4.686	3.755	4.156
CCSD(T)/aqz//B3LYP/adz	4.294	4.707	3.789	4.189
CCSD(T)/CBS//B3LYP/adz	4.309	4.721	3.809	4.210
CCSD(T)/adz//MP2/adz	4.137	4.549	3.642	4.043
CCSD(T)/atz//MP2/adz	4.272	4.686	3.752	4.153
CCSD(T)/aqz//MP2/adz	4.293	4.705	3.785	4.186
CCSD(T)/CBS//MP2/adz	4.306	4.723	3.799	4.212
CCSD(T)/adz//MP2/atz	4.132	4.549	3.635	4.048
CCSD(T)/atz//MP2/atz	4.268	4.685	3.741	4.154
CCSD(T)/aqz//MP2/atz	4.290	4.707	3.775	4.187
CCSD(T)/CBS//MP2/atz	4.309	4.722	3.813	4.214
G2MP2	4.376		3.840	
CBS-Q	4.334		3.793	
SRP-PM3	4.238	4.625	3.880	4.211
SRP−MSINDO	4.223	4.609	3.765	4.129
experiment (from ref 27)	4.176		3.812	
experiment (from ref 30)	4.361		3.889	
experiment (from ref 28)	4.382		3.909	
experiment (from ref 29)	4.383		3.905	

[a] The abbreviations adz, atz, aqz, and CBS represent aug-cc-pvdz, aug-cc-pvtz, aug-cc-pvqz, and complete-basis set, respectively. ZPE = zero-point energy.

the C_2H_6 molecules and large basis sets are impossible at this time, we therefore use our CCSD(T) results here as a benchmark to calibrate the accuracy of other lower-cost methods. Figure 3 shows that MP2 provides dissociation energies in closer agreement with CCSD(T) data, but B3LYP better matches the CCSD(T) behavior throughout the dissociation curves. The PM3 curves fall far below the first-principles estimates, as anticipated from the BDEs reported in Table 2. In addition, PM3 predicts a C−C bond that is notably stiffer than the first-principles calculations. MSINDO, although showing an asymptotic behavior more similar to first-principles methods than PM3, displays yet much stiffer C−C and C−H bonds than both ab initio and PM3 methods.

To improve the accuracy of the PM3 and MSINDO Hamiltonians, we have reoptimized the parameters of the C and H atoms so that the Hamiltonians better reproduce the CCSD(T)/aug-cc-pvtz data shown in Figure 3. Operationally, we have achieved this by minimizing the difference between the CCSD(T)/aug-cc-pvtz energies and the PM3 or MSINDO results using a nonlinear least-squares procedure. Aside from considering the CCSD(T)/aug-cc-pvtz points shown in Figure 3 in the reoptimization of the PM3 and MSINDO parameters, we have included points other than the bond-dissociation curves of the C_2H_6 PES that are likely explored in the dynamics simulations. These points correspond to a molecular-dynamics simulation of C_2H_6 in which 2 quanta of excitation are assigned initially to each of the normal modes. This trajectory of highly vibrationally excited C_2H_6 is integrated for 10 ps, using the B3LYP/6-31+G* method. Geometries are recorded every 100 fs, and their energies are calculated at the MP2/aug-cc-pvdz level. The resulting 100 ab initio points are included in the fit to better represent Ar + C_2H_6 trajectories in which there is a large translational → vibrational energy transfer, but no dissociation occurs.

Figure 4 shows the estimates of the specific-reaction-parameters PM3 and MSINDO Hamiltonians that best match the CCSD(T)/aug-cc-pvtz//B3LYP/aug-cc-pvdz data along the dissociation energy curves, and the MP2/aug-cc-pvdz energies of the high-internal-energy C_2H_6 trajectory previously mentioned. Two points are worth mentioning. First, the SRP Hamiltonians are a great improvement over the original Hamiltonians. For instance, Table 2 shows that the dissociation energies of both the C−H and C−C bonds have been improved by ∼1 eV for SRP-PM3, and by 0.2−0.4 eV for SRP-MSINDO, and all SRP values are in good agreement with experiments. Second, the SRP-PM3 and SRP-MSINDO Hamiltonians do not perfectly match the CCSD(T) data throughout the dissociation curves. The differences are more noticeable in the region of the curves prior to the asymptote. We note that our parameter-optimization procedure generates various sets of parameters with different agreement with the higher-level calculations used as a reference. Some of these sets of parameters showed a closer match with the CCSD(T) data in the region of the curve prior to the asymptote than that observed in Figure 4. However, the dissociation energies were not described as well. Therefore, our choice of the SRP Hamiltonians shown in Figure 4 was based on a compromise between accuracy in the asymptote and elsewhere in the PES. The root-mean-square (RMS) deviations between the ab initio and SRP points belonging to the dissociation-energy curves are 0.22 and 0.20 eV, respectively, for SRP-PM3 and SRP-MSINDO.

In summary, we have been able to generate SRP-PM3 and SRP-MSINDO Hamiltonians for treating C_2H_6 dissociation with accuracy that is comparable to that of a mainstream first-

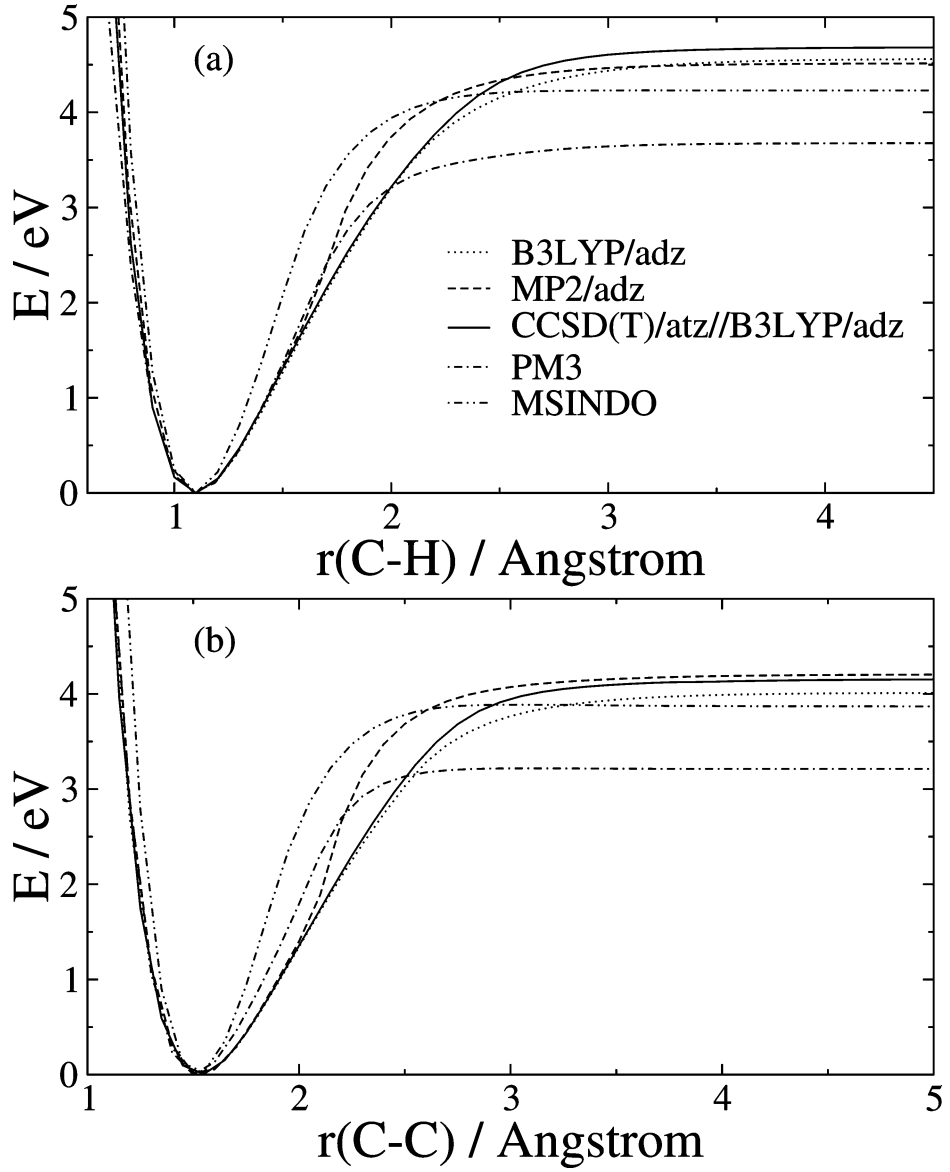

Figure 3. Calculated minimum-energy dissociation curves for the (a) C−H and (b) C−C bonds in the C_2H_6 molecule. The acronyms "adz" and "atz" represent the aug-cc-pvdz and aug-cc-pvtz basis sets, respectively. CCSD(T)/atz//B3LYP/adz corresponds to CCSD(T)/aug-cc-pvtz single-point calculations using geometries optimized at the B3LYP/aug-cc-pvdz level.

principles methods, but which require orders of magnitude less computational effort. Although there are some differences between our best ab initio estimates (CCSD(T)) and the SRP Hamiltonians, these occur in a region of the potential-energy curve that is difficult to describe by relatively low-cost electronic-structure methods, such as MP2. In fact, the overall performance of our SRP Hamiltonians is superior to MP2/aug-cc-pvdz calculations throughout the dissociation energy curves. We use these SRP Hamiltonians to represent the C_2H_6 intramolecular potential in the Ar + C_2H_6 trajectory calculations described later.

We now turn our attention to C_2F_6. Electronic-structure calculations of the C−F and C−C BDEs are shown in Table 3. As with C_2H_6, the results obtained with the original PM3 Hamiltonian are removed from experiments and first-principles theories. However, in contrast to C_2H_6, the C−F and C−C PM3 bond energies are not underestimated by similar amounts. Instead, the error in the C−F dissociation energy is ∼1 eV, while the error in the C−C bond is >2 eV. The underestimation of the C−C bond energy by the AM1 method is even larger. MSINDO provides dissociation energies in slightly better agreement with experiments, but the difference with experiments for the C−C channel is still almost 2 eV. B3LYP calculations also underestimate experiments. Interestingly, the error in the C−F BDE is quite large (∼0.5 eV), which suggests that describing a C−F bond is more difficult than a C−H bond. MP2 reproduces the experimental C−C BDE well, but overestimates the energy of the C−F bond. An extrapolation of the MP2 C−F bond energies to the complete basis-set limit results in a bond energy that is ∼0.25 eV above that of the experiments. The C−F and C−C BDEs calculated at the CCSD(T)/aug-cc-pvdz level utilizing B3LYP/aug-cc-pvdz geometries and frequencies are in good agreement with experiments for C−C, but underestimate them for C−F. An increase in the basis set to aug-cc-pvtz brings the CCSD(T) estimates closer to the experiment. Although we cannot afford aug-cc-pvqz calculations with this method for C_2F_6, we can infer from the CCSD(T)/aug-cc-pvdz and aug-cc-pvtz results that an extrapolation of CCSD(T) energies to the complete basis-set limit would match the experiments quite accurately. The conclusion from these calculations is that, although in C_2H_6, the C−H and C−C bond energies calculated with the B3LYP and MP2 methods are in

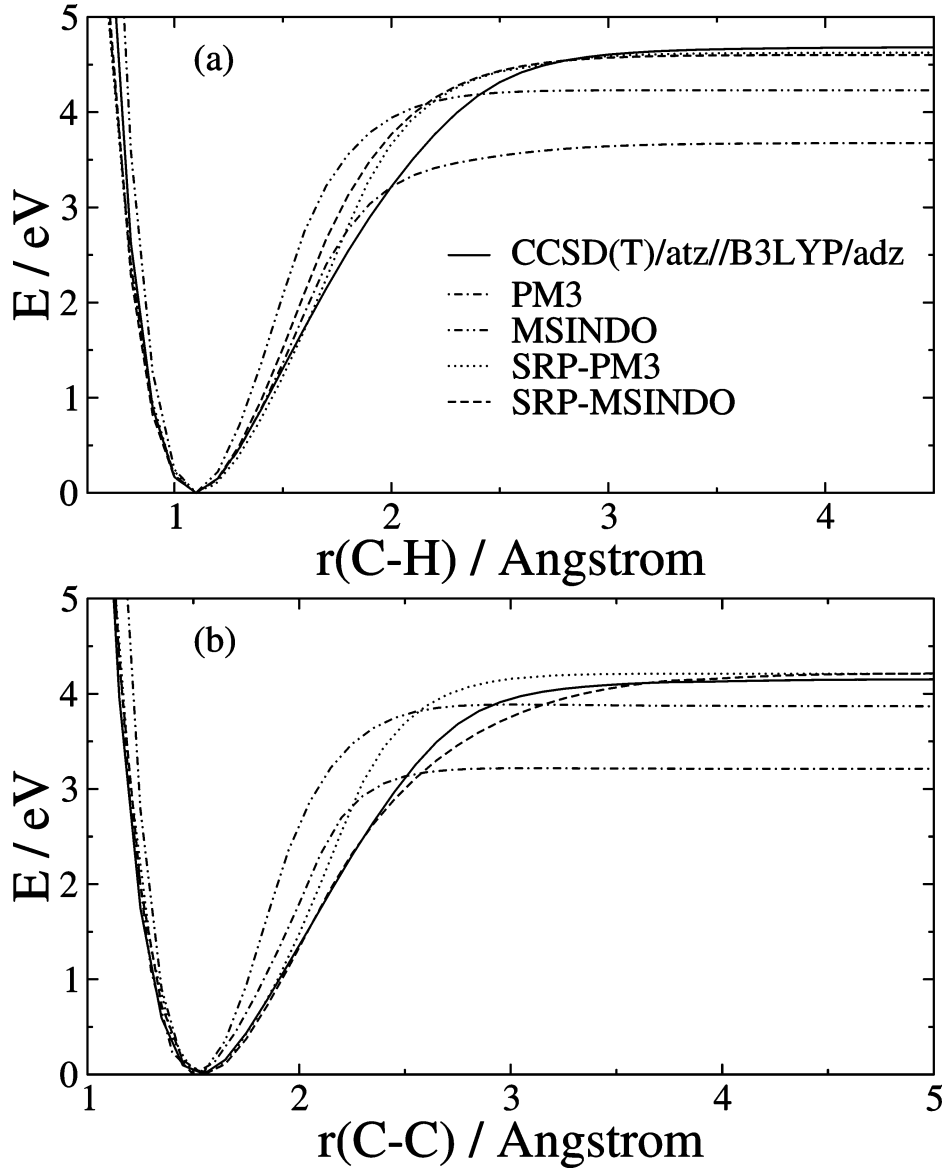

Figure 4. Calculated minimum-energy dissociation curves for the (a) C−H and (b) C−C bonds in the C_2H_6 molecule. The figure compares the SRP Hamiltonians derived in this work with the original Hamiltonians and the ab initio data used for reparameterization. The term "CCSD(T)/atz//B3LYP/adz" corresponds to CCSD(T)/aug-cc-pvtz single-point calculations using geometries optimized at the B3LYP/aug-cc-pvdz level.

good agreement with experiments, CCSD(T) theory and very large basis sets are needed to describe the dissociation energy of the C−F bond in C_2F_6 accurately.

Figures 5a and 5b respectively show the dissociation-energy curves for the C−F and C−C bonds in C_2F_6 predicted by various computational models. As with C_2H_6, the curves represent relaxed scans of the C−F and C−C bonds calculated using an unrestricted reference and mixing the initial lowest unoccupied molecular orbital (LUMO) and highest occupied molecular orbital (HOMO). For the C−F dissociation curve, we see that, at intermediate and long distances, the CCSD(T) results are between MP2 and B3LYP, with noticeable differences in the shapes of the three curves. The results are similar for the C−C dissociation, but B3LYP parallels CCSD(T) throughout most of the curve. The PM3 data display a C−F bond that is stiffer but weaker than predicted by first-principles calculations. Larger errors are observed in the PM3 C−C dissociation curve, where, in addition to an asymptote that is too low, one can see a noticeable overestimation of the equilibrium C−C distance (1.608 Å vs 1.553 Å at the B3LYP/aug-cc-pvdz level). MSINDO matches PM3 in the C−F dissociation energy curve, and describes slightly better the C−C dissociation energy. However, Figure 5b shows that the C−C bond in MSINDO is noticeably stiffer than predicted by first-principles calculations.

To improve the PM3 and MSINDO Hamiltonians for the C_2F_6 molecule, we have modified the original parameters so that the Hamiltonians reproduce the CCSD(T) points of the C−C and C−F dissociation curves shown in Figure 5. In addition to these 102 points (51 in each curve), we have included 112 points that belong to a C_2F_6 trajectory started with 4 quanta of excitation in each normal mode. We integrated such trajectory using the B3LYP/6-31G** method for 1 ps, and we recorded 112 sets of coordinates equally spaced in time. CCSD(T)/aug-cc-pvdz single-point calculations were used to refine the energies before including the points in the reoptimization of the semiempirical Hamiltonians. After a nonlinear least-squares optimization of the semiempirical parameters, we have chosen SRP-PM3 and SRP-MSINDO Hamiltonians with best behavior throughout all of the reference ab initio points. The C−F and C−C BDE curves predicted by these Hamiltonians are plotted against CCSD(T) and original PM3 and MSINDO data in Figure 6. One can see that the BDEs of the SRP Hamiltonians are greatly improved,

TABLE 3: Experimental and Calculated C_2F_6 Bond Dissociation Energies[a]

	bond dissociation energy, BDE (eV)			
	C_2F_5-F		CF_3-CF_3	
	with ZPE	classical (without ZPE)	with ZPE	classical (without ZPE)
PM3	4.430	4.565	2.067	2.200
AM1	4.002	4.123	0.929	1.059
MSINDO	4.509	4.628	2.371	2.496
B3LYP/adz	5.035	5.163	3.803	3.941
B3LYP/atz	5.091	5.220	3.711	3.846
MP2/adz	5.435	5.563	4.277	4.421
MP2/atz//MP2/adz	5.671	5.799	4.301	4.446
MP2/aqz//MP2/adz	5.726	5.854	4.305	4.449
MP2/CBS//MP2/adz	5.766	5.893	4.307	4.452
CCSD(T)/adz//B3LYP/adz	5.129	5.257	4.221	4.358
CCSD(T)/atz//B3LYP/adz	5.347	5.474	4.210	4.348
G2MP2	5.514		4.286	
CBS-Q	5.551		4.365	
SRP-PM3	5.053	5.181	3.928	4.074
SRP−MSINDO	5.189	5.282	4.189	4.259
experiment (from ref 27)			4.180	
experiment (from ref 28)	5.521		4.280	

[a] The abbreviations adz, atz, aqz, and CBS represent aug-cc-pvdz, aug-cc-pvtz, aug-cc-pvqz, and complete-basis set, respectively. ZPE = zero-point energy.

with respect to the original Hamiltonians (see also Table 3). The shape of the dissociation-energy curves is also improved, but SRP-MSINDO does not reproduce the CCSD(T) data in the region of the C−F curve prior to the asymptote as well as SRP-PM3 does. Note also that reparameterization is able to correct the C−C equilibrium distance in SRP-PM3. The RMS deviation between the ab initio and SRP points belonging to the dissociation-energy curves are 0.21 and 0.15 eV, respectively, for SRP-PM3 and SRP-MSINDO.

We have verified that the performance of the SRP potentials is adequate for situations in which the Ar atom is close to the molecules by performing ab initio calculations of selected integration steps of actual trajectories integrated with the SRP Hamiltonians. The differences between ab initio points and SRP Hamiltonians are similar to those of the points included in the fit, giving confidence that the SRP Hamiltonians are well-behaved in actual collisions.

The PM3 and MSINDO SRP parameters for the C_2H_6 and C_2F_6 molecules are listed in Tables 4 and 5, respectively. We have used the SRP-PM3 and SRP-MSINDO Hamiltonians for C_2F_6 in conjunction with the Ar−C_2F_6 intermolecular potential previously described to integrate classical trajectories for Ar + C_2F_6 collisions. In the next section, we describe trajectory calculations for collisions of the Ar atom with C_2H_6 and C_2F_6 molecules at high energies.

Dynamics Simulations of Ar + C_2H_6 and Ar + C_2F_6 Collisions

Computational Details. Using the hybrid PES previously described, we have performed classical-trajectory calculations of collisions of the Ar atom with C_2H_6 and C_2F_6 molecules at high energies. We have integrated batches of 2000−3000 trajectories at collision energies in the range of 5−12 eV. Operationally, we have interfaced a predictor-corrector algorithm that solves the equations of motion with the GAMESS[35] and MSINDO codes to obtain, "on the fly", the potential energy and derivatives for C_2X_6 (where X = H, F) with the SRP-PM3 and SRP-MSINDO Hamiltonians, respectively. In the quantum-mechanical calculation of the intramolecular energy with the SRP Hamiltonians, we have used an unrestricted reference and a fresh guess of the initial orbitals in which the HOMO and LUMO are mixed at each integration step. We note that the orbital mixing must be performed at each integration step to ensure the correct dissociation limit. This makes a difference with the common procedure in direct-dynamics calculations of using the converged orbitals of the previous step as a guess for the current step, and increases the computational expenditure in the current calculations. An additional subroutine calculates the Ar−molecule intermolecular potential and derivatives using the Buckingham potentials previously described.

We have started the trajectories at an initial separation of 15 au between the Ar atom and the center of mass of the molecules, which possess zero-point energy (ZPE) motion. This distance is sufficiently long that the interaction energy between the atom and molecule is negligible, with respect to the total initial energy. We have solved the classical equations of motion each 10 au (0.24 fs) and 30 au (0.72 fs) for Ar + C_2H_6 and Ar + C_2F_6, respectively. With these integration steps, the total energy is conserved, on the average, to better than 0.01 eV for all semiempirical Hamiltonians at all energies. Individual trajectories that did not conserve energy to 0.4 eV were discarded from the analysis. We have used several criteria for stopping the trajectories. If no bond breakage happens, the trajectories are stopped when either of the Ar−C distances reaches 30 au. If collision-induced dissociation occurs in the SRP-MSINDO calculations, the trajectories are stopped when the distance between the two atoms of the broken bond reaches 15 au. We tried to use an identical criterion for the SRP-PM3 calculations, but found that the self-consistent field (SCF) procedures available in GAMESS frequently failed to converge for long distances between the recoiling radicals. Although we tried different SCF convergers available in GAMESS, we were unsuccessful in finding a procedure that robustly achieved convergence. After a careful study, we consider that bond breakage happens when a C−X (for X = H, F) or C−C bond reaches 7.0 au (3.7 Å). Note that, at these distances, the interaction energy between the separating fragments is <1% of the corresponding BDE. In some cases, particularly at high collision energies, the SCF procedure fails to converge for SRP-PM3 calculations when a C−C or C−X (for X = H, F) bond is elongating, but still has not reached 3.7 Å. In these cases,

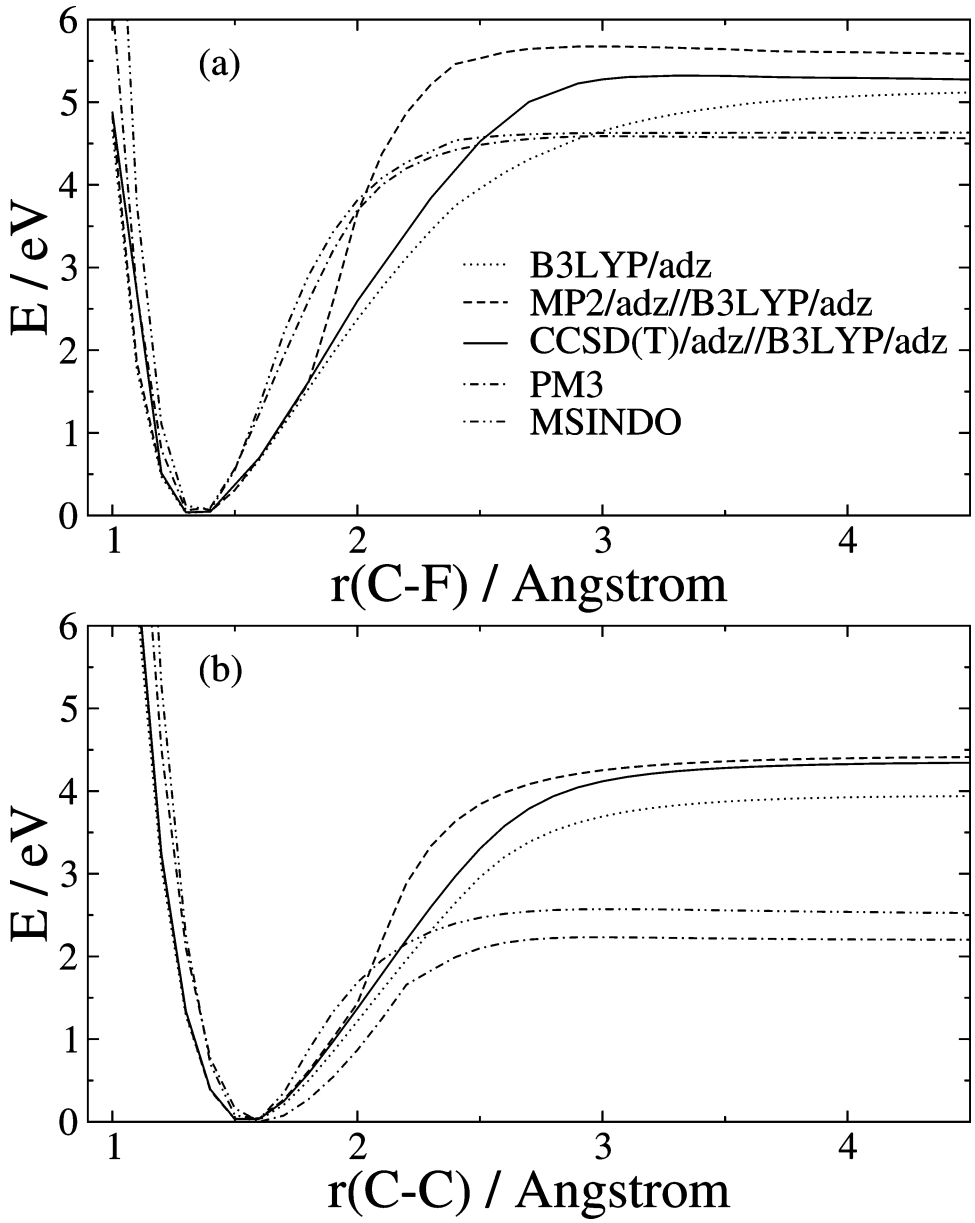

Figure 5. Calculated minimum-energy dissociation curves for the (a) C−F and (b) C−C bonds in the C_2F_6 molecule. The acronym "adz" represents the aug-cc-pvdz basis set. The term "CCSD(T)/adz//B3LYP/adz" corresponds to CCSD(T)/aug-cc-pvdz single-point calculations using geometries optimized at the B3LYP/aug-cc-pvdz level.

we examine the internuclear distances of the molecule in the step prior to the SCF failure, and if a C−X or C−C bond is >3.0 Å, and the trajectory has conserved energy prior to the SCF failure, the trajectory is assumed to be reactive. The percentages of trajectories in which the SCF procedure fails and do not satisfy the internuclear-distance criteria previously described are 4% and 12% of the total number of reactive trajectories at $E_{coll} = 12$ eV in Ar + C_2H_6 and Ar + C_2F_6, respectively.

Energy Transfer. A main goal of this study is to investigate the possibility of collision-induced dissociation (CID) in hyperthermal collisions of the Ar atom with C_2H_6 and C_2F_6 molecules. Regardless of whether CID is a result of a C−X (for X = H, F) or C−C bond breakage, we can separate CID into two types: prompt and delayed. Here, we define prompt CID as a process whereby the molecule dissociates while the Ar projectile is still in the vicinity of the molecule after collision (maximum r(Ar−C) < 30 au). In delayed CID, the Ar−molecule collision results in molecular excitation above the lowest-energy BDE (C−C in both C_2H_6 and C_2F_6). The excitation energy is initially shared by several molecular degrees of freedom, but after some time, it accumulates in a stretching mode and the molecule dissociates. One difference between prompt and delayed CID is that, while prompt CID can be considered to be a bimolecular process, delayed CID is unimolecular. Another difference is that prompt CID occurs on the subpicosecond time scale, but delayed CID can occur anywhere starting in the picosecond time scale and extending well beyond the nanosecond time scale. Our study can only quantify directly prompt CID, because direct-dynamics simulations beyond the picosecond time scale are unwieldy, even with semiempirical Hamiltonians. However, we can still partially investigate delayed CID by analyzing trajectories in which the molecule receives more energy than required to break a bond. Some of these trajectories result in prompt CID, as we will describe later. In the remaining trajectories, the highly excited molecules will either dissociate after some time (delayed CID)

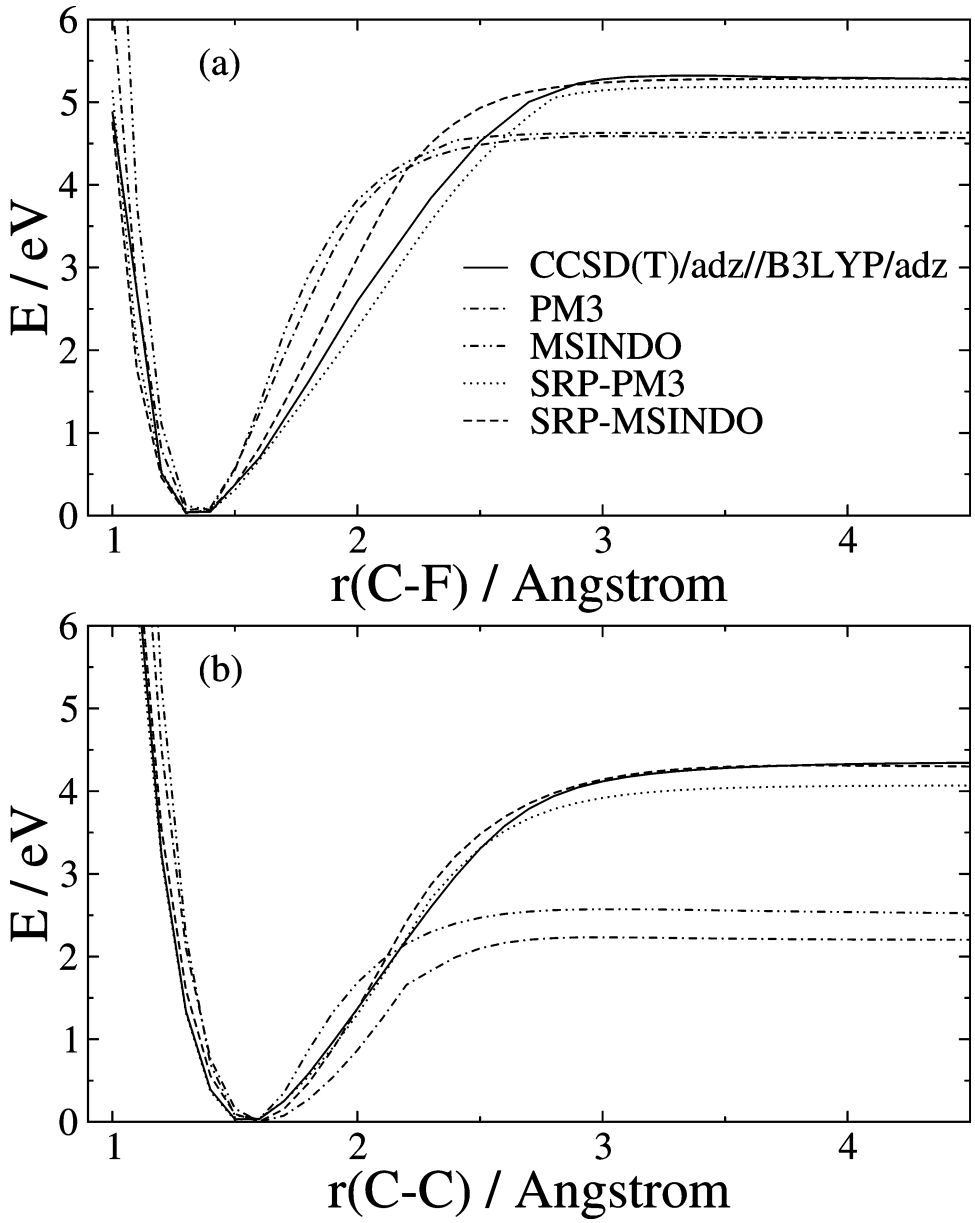

Figure 6. Calculated minimum-energy dissociation curves for the (a) C−F and (b) C−C bonds in the C_2F_6 molecule. The figure compares the SRP Hamiltonians derived in this work with the original Hamiltonians and the ab initio data used for reparameterization. The term "CCSD(T)/adz//B3LYP/adz" corresponds to CCSD(T)/aug-cc-pvdz single-point calculations using geometries optimized at the B3LYP/aug-cc-pvdz level.

or continue vibrating without dissociating until they are deactivated via secondary collisions.

Figure 7 shows the calculated excitation functions (cross section versus collision energy) of trajectories in which more energy than required to break a bond is transferred to the molecule during the collision. The minimum energy to break a bond is provided by the classical dissociation energy of the weakest bond for each Hamiltonian. In all cases, the weakest bond is C−C, and its classical BDEs are 4.211 and 4.129 eV for SRP-PM3 and SRP-MSINDO calculations in Ar + C_2H_6, and 4.074 and 4.259 eV for SRP-PM3 and SRP-MSINDO calculations of Ar + C_2F_6. Figure 7 reveals that energy transfer to C_2F_6 is much more important than to C_2H_6. The enhanced energy transfer to the fluorinated species stems from the lower frequencies in the heavier species, as has been well-described previously.[36] At large collision energies, the cross section of trajectories yielding C_2F_6 above the lowest-energy dissociation limit is more than three times larger than that for C_2H_6. In addition, the minimum collision energy at which C_2F_6 molecules possess more energy than required to break a bond also occurs at lower energies than that for C_2H_6. Specifically, collisions of Ar + C_2F_6 at 5 eV can produce C_2F_6 with internal energy over the dissociation limit, but 6 eV are necessary in the case of C_2H_6. This is quite remarkable, because the classical C−C BDEs in C_2H_6 and C_2F_6 are similar (see Tables 2 and 3). The cross sections of trajectories that excite C_2F_6 and C_2H_6 above their dissociation limit at $E_{coll} = 11$ eV (relative collision energy in the direction of travel in LEO) are sizable. This result indicates that, in principle, it is physically possible that Ar atoms present at low altitudes in LEO induce C−C bond breakage in the hydrocarbon polymers acting as thermal blankets of the surface of spacecraft operating in that region of space.

Another interesting point in Figure 7 is that the cross section provided by the SRP-PM3 and SRP-MSINDO Hamiltonians are similar in each system. Particularly, at the highest energies studied here, the SRP-PM3 and SRP-MSINDO results overlap within statistical uncertainty for both Ar + C_2F_6 and Ar + C_2H_6. Figures 4 and 6 indicate that, although the dissociation limits

TABLE 4: Original and SRP PM3 Parameters for the H and C, and F and C, Atoms for the Ar + C_2H_6, and Ar + C_2F_6, Reactions, Respectively

	Ar + C_2H_6				Ar + C_2F_6			
	H		C		F		C	
parameter	original	SRP	original	SRP	original	SRP	original	SRP
U_{SS}	−13.0733	−11.9680	−47.2703	−45.3483	−110.4353	−116.8723	−47.2703	−41.1785
U_{PP}			−36.2669	−35.1590	−105.6850	−92.5569	−36.2669	−29.6077
β_S	−5.6265	−6.0296	−11.9100	−11.4009	−48.4059	−55.2842	−11.9100	−15.7707
β_P			−9.8028	−9.2237	−27.7446	−18.2438	−9.8028	−7.760
ζ_S	0.9678	1.0364	1.5651	1.5480	4.7086	4.0130	1.5651	1.5846
ζ_P			1.8423	1.7245	2.4912	2.3903	1.8423	1.5269
a	3.3564	3.1067	2.7078	2.8032	3.3589	3.2105	2.7078	2.9856
G_{SS}	14.7942	13.9190	11.2007	10.2092	10.4967	12.3967	11.2007	8.8784
G_{SP}			10.2650	10.5867	16.0737	17.3529	10.2650	7.2889
G_{PP}			10.7963	9.0407	14.8173	7.6594	10.7963	12.1681
G_{P2}			9.0426	9.9405	14.4184	12.5607	9.0426	9.5084
H_{SP}			2.2910	2.2201	0.7276	1.1337	2.2910	1.9942

TABLE 5: Original and SRP MSINDO Parameters for the H and C, and F and C, Atoms for the Ar + C_2H_6, and Ar + C_2F_6, Reactions, Respectively

	Ar + C_2H_6				Ar + C_2F_6			
	H		C		F		C	
parameter	original	SRP	original	SRP	original	SRP	original	SRP
ζ_s^U	1.0060	0.8118	1.6266	1.4688	2.3408	2.3113	1.6266	1.2089
ζ_p^U			1.5572	1.1624	2.2465	1.4116	1.5572	1.1874
ζ_s	1.1576	1.2429	1.7874	2.2220	2.4974	2.2030	1.7874	1.7456
ζ_p			1.6770	1.3112	2.3510	2.2636	1.6770	1.3116
I_s	0.5000	0.4003	0.8195	0.7447	2.0238	1.3218	0.8195	0.6791
I_p			0.3824	0.3826	0.6868	0.5170	0.3824	0.3890
$-\epsilon_{1s}$			10.430	9.6853	25.190	33.715	10.430	10.686
τ_{1s}			5.0830	5.8720	8.6043	9.3827	5.0830	8.3217
K_s	0.1449	0.0665	0.0867	0.0664	0.1769	0.1070	0.0867	0.1178
K_p					0.0127	0.0090	0.0478	0.0293
k_1	0.3856	0.0514	0.4936	0.7393				
k_2					0.1059	0.1382	0.6776	0.4734

predicted by each SRP Hamiltonian in each molecule are similar, the shapes of the dissociation curves differ in some cases. For instance, the C−C bond in the SRP-PM3 Hamiltonian for C_2H_6 is notably stiffer than in the SRP-MSINDO Hamiltonian. Conversely, the C−F bond is stiffer for SRP-MSINDO than for SRP-PM3 in C_2F_6. Therefore, the good level of agreement between the SRP-PM3 and SRP-MSINDO results in Figure 7 suggests that energy transfer above the dissociation limit is relatively insensitive to the intramolecular potential.

Collision-Induced Dissociation Cross Sections. Figure 7 displays the cross section for Ar + C_2H_6 and Ar + C_2F_6 collisions in which the amount of energy transferred to the molecule is above the lowest-energy molecular dissociation limit. As mentioned previously, the fate of these collisions is 2-fold. The highly excited molecules can dissociate while the recoiling Ar atom is still in the vicinity of the molecule (prompt CID), or it can remain excited after the Ar atom has departed the interaction region, unimolecularly dissociating or not. Figure 8 presents the cross sections of prompt CID only. There are two possible reaction channels: C−C bond cleavage and C−X (for X = H, F) cleavage. The cross sections for C−C breakage clearly dominate over those for C−X breakage at all energies studied here, and with all intramolecular potentials. In addition, the threshold for C−C breakage occurs at lower collision energies than that for C−X. The obvious reason for the difference in the threshold is the lower dissociation energy of the C−C bond, with respect to the C−X bond in C_2H_6 and C_2F_6. At energies well above the threshold, one would expect the C−X cross section to dominate, because of purely statistical reasons (the ratio of C−X bonds to C−C bonds is 6:1). However, the result of our chemical dynamics simulations indicate that C−C dominates, even at the highest collision energies studied here (12 eV). This result suggests that the C−C bond is the weak link of the C_2X_6 molecules. Another reason why C−C breakage dominates C−X breakage is its larger cone of acceptance at energies up to 12 eV. For instance, for Ar + C_2F_6 collisions at E_{coll} = 12 eV, the maximum impact parameter that leads to C−C breakage is 1.0 au larger than that which leads to C−F breakage with SRP-PM3 (4.5 vs 3.5 au, respectively). The results are similar for SRP-MSINDO. For Ar + C_2H_6 collisions at E_{coll} = 12 eV with SRP-PM3, the maximum impact parameter is 3.2 au for C−C cleavage and 2.7 au for C−H cleavage.

An interesting result is that the prompt CID cross sections for the SRP-PM3 and SRP-MSINDO Hamiltonians differ in both Ar + C_2H_6 and Ar + C_2F_6. For Ar + C_2H_6, the SRP-MSINDO C−C breakage cross section is larger than that of SRP-PM3. Conversely, the SRP-MSINDO cross section for C−H breakage is negligible, but that with SRP-PM3 is sizable. These findings can be understood based on the shapes of the dissociation energy curves shown in Figure 4. In Figure 4b, we see that the SRP-PM3 C−C BDE curve is much tighter than that for SRP-MSINDO. Although the C−C dissociation energies are similar, the looser curve of SRP-MSINDO is easier to surmount, resulting in an enhanced C−C breakage cross section. In Figure 4a, we see that the SRP-MSINDO C−H dissociation curve is only slightly tighter than that of SRP-PM3. Therefore, it seems that, while trajectories integrated using the SRP-PM3 Hamiltonian face dissociative potentials of comparable steepness for the C−C and C−H bonds, the looser character of the C−C bond in SRP-MSINDO draws most of the trajectories toward C−C dissociation.

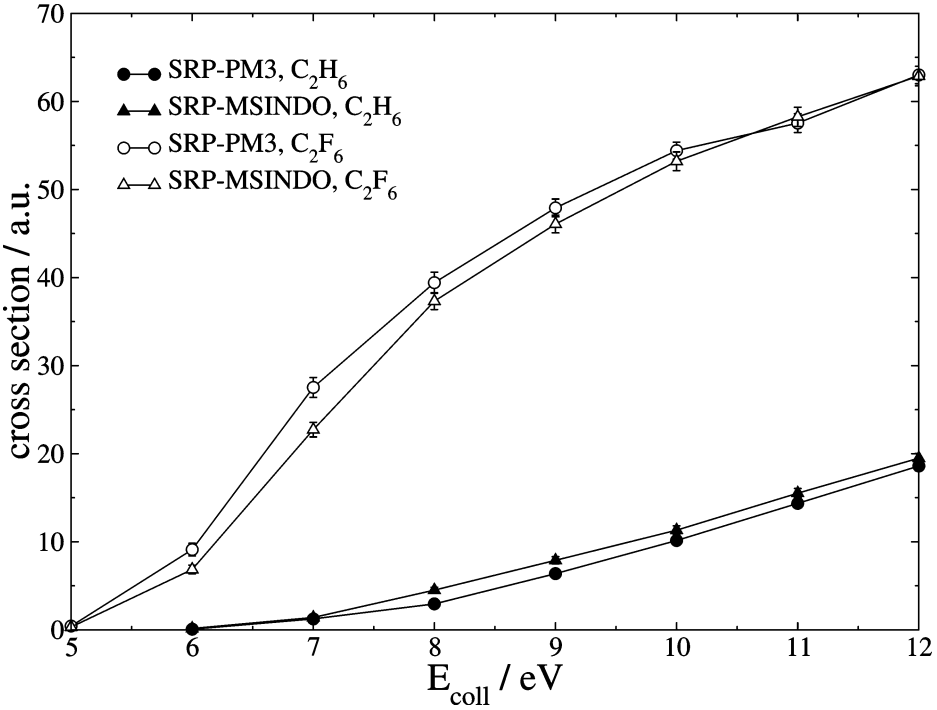

Figure 7. Cross sections of Ar + C_2H_6 and Ar + C_2F_6 collisions in which energy transfer above the C−C bond dissociation energy (BDE) occurs, as a function of collision energy.

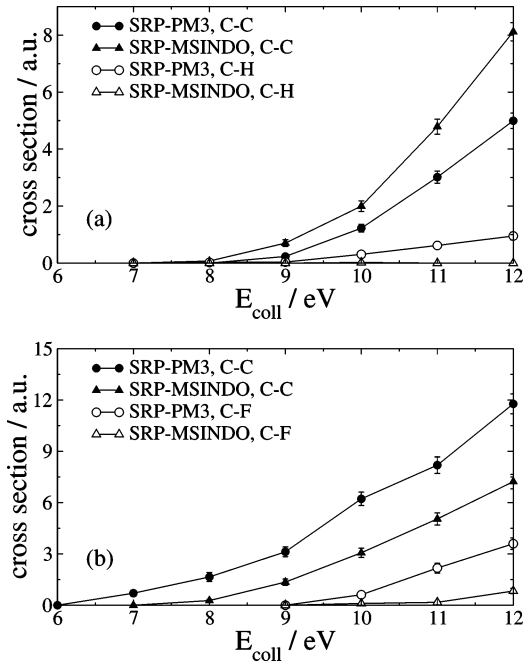

Figure 8. Excitation functions for prompt collision-induced dissociation in Ar + C_2X_6 hyperthermal collisions: (a) Ar + C_2H_6 collisions and (b) Ar + C_2F_6 collisions.

Contrary to the trend observed in Ar + C_2H_6, the C−C CID cross section for trajectories integrated with the SRP-PM3 Hamiltonian is larger than that with SRP-MSINDO in Ar + C_2F_6 collisions. Figure 6b indicates that the C−C BDE curve according to SRP-PM3 is slightly looser than that of SRP-MSINDO. In addition, the dissociation energy is slightly lower for SRP-PM3 than for SRP-MSINDO. The combination of these two factors favors the dissociation of the C−C bond in the SRP-PM3 trajectories. Regarding the C−F CID cross sections, Figure 8 shows that the SRP-PM3 cross sections are larger than the SRP-MSINDO cross sections. Looking at Figure 6a, we can understand this trend based on the increased stiffness of the C−F bond according to SRP-MSINDO with respect to SRP-PM3.

Irrespective of the differences between the intramolecular potentials used in this work, we see that the Ar atom can break bonds in hydrocarbons at collision energies well below those accessible in LEO. On average, fluorinated hydrocarbons seem to undergo CID upon collisions with hyperthermal Ar atoms more frequently that regular hydrocarbons.

Reaction Mechanism. An attractive capability of the classical-trajectory method is that it is able to track the positions of the nuclei during the collisions and to help decipher the reaction mechanism. To describe the mechanisms for prompt CID, we have studied the geometries explored by the system in reactive trajectories. In particular, we have studied the distance between the Ar atom and the center of mass of the molecule (RSH), and the angle (θ) between the vector joining the Ar atom and the center of mass of the molecule and the C−C internuclear vector. The RSH distance is 15 au at the beginning of the trajectories. As the trajectories proceed, the RSH distance becomes smaller until it reaches a minimum value, which determines the inner turning point of the trajectories. After that, the RSH distance increases as products separate. The angle θ is initially distributed uniformly between 0° and 180°, as required for a complete sampling of the configuration space. However, analysis of reactive trajectories reveals that, as the trajectories proceed, some θ values are more efficient than others, in regard to producing CID.

Figure 9 shows the probability distributions of the θ angle at the inner turning point of the collisions that result in CID in Ar + C_2F_6 at E_{coll} = 12 eV with SRP-PM3. The probability distributions of C−C and C−F CID are plotted separately. The figure shows that the most probable θ angle that leads to C−C CID is ∼90°. This corresponds to "side-on" collisions in which the Ar atom approaches perpendicular to the C−C axis (see inset in Figure 9). Trajectory animation reveals that this approach is effective in producing C−C dissociation, because the Ar atom

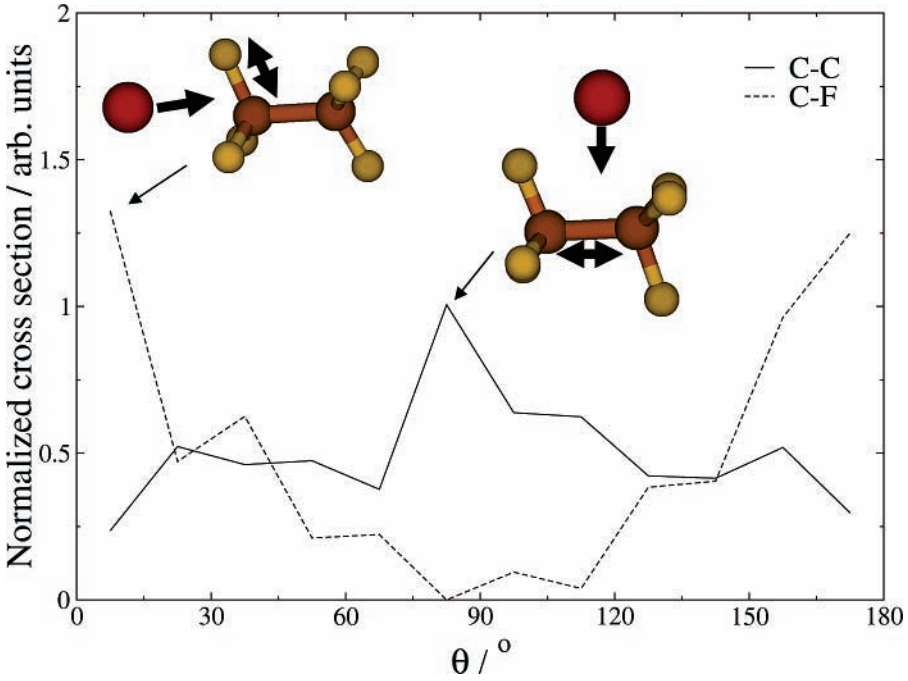

Figure 9. Distributions of the angle formed between the Ar−molecule center of mass vector and C−C internuclear vector at the inner turning point of reactive Ar + C_2F_6 trajectories. The results correspond to SRP-PM3 calculations at a collision energy of $E_{coll} = 12$ eV.

pushes the two CF_3 moieties in opposite directions, which results in C−C bond breakage. On the other hand, θ angles closer to 0° or 180° are more efficient in producing C−F bond dissociation. These angles are representative of "head-on" collisions, in which the Ar atom approaches more collinearly to the C−C bond. Trajectory animation reveals that C−F breakage occurs when the Ar atom tries to insert in a C−F bond (see inset in Figure 9). This approach pushes the C and F atoms in opposite directions, resulting in the dissociation of a C−F bond.

Concluding Remarks

We have characterized the intermolecular potential between the Ar atom and regular and perfluorinated hydrocarbons by developing highly accurate ab initio calculations of selected approaches of the Ar atom to the CH_4 and CF_4 molecules at the fp-CCSD(T)/CBS level. The calculations cover interaction energies up to 17 eV. We have derived pairwise analytical potentials that reproduce the high-level ab initio data and verified that they are applicable to study Ar + C_2H_6 and Ar + C_2F_6 collisions at high energies.

We have also investigated the intramolecular potential of the C_2H_6 and C_2F_6 molecules using high-level ab initio theory. The bond-dissociation energies of the C_2H_6 molecule are well-described by all of the first-principles methods used here (B3LYP, MP2, and CCSD(T)). On the other hand, only CCSD(T) theory is able to reproduce the experimental dissociation energies for C_2F_6 accurately, with MP2 overestimating the experiments and B3LYP underestimating them. We have used CCSD(T) data in both systems to improve the PM3 and MSINDO semiempirical Hamiltonians for the C_2H_6 and C_2F_6 molecules via reoptimization of the parameters included in the Hamiltonians. The specific-reaction-parameter Hamiltonians reproduce the experimental dissociation energies quite well and show a reasonable behavior in other regions of the potential-energy surface (PES).

Using these intermolecular and intramolecular PES, we have conducted classical-trajectory calculations of Ar + C_2H_6 and Ar + C_2F_6 encounters at collision energies ranging from 5 eV to 12 eV. Trajectory analysis reveals that the cross sections for energy transfer above the lowest-energy dissociation limit is sizable, with energy transfer to C_2F_6 being much more efficient than energy transfer to C_2H_6. This large amount of energy transfer results in prompt collision-induced dissociation (CID) in both C_2F_6 and C_2H_6. C−C dissociation is more important than C−F or C−H dissociation, but both channels are open at high energies. Although there are some differences in the prompt CID cross sections predicted by the SRP-PM3 and SRP-MSINDO Hamiltonian, both Hamiltonians provide overlapping cross sections for energy transfer. This finding indicates that, although energy transfer seems relatively insensitive to the intramolecular potential, the shape of this potential has a larger role in the dynamics ensuing energy transfer.

The key result of this work is that the Ar atom can break C−C bonds at collision energies accessible in low Earth orbit (LEO). Until now, most of the efforts that have been made to understand the degradation of the polymer coating of spacecraft surfaces in LEO at a molecular level have concentrated on $O(^3P)$ reactivity, because this is the most abundant species in LEO. However, recent experiments indicate that fluorinated polymers are inert to hyperthermal $O(^3P)$. This paper puts forward an alternative mechanism for degradation of hydrocarbon polymers based on efficient energy transfer, ensuing collision with nonreactive species heavier than $O(^3P)$, which ultimately leads to dissociation.

Current efforts in our group are directed at unveiling the possibility of CID in collisions of hyperthermal Ar atoms with condensed-phase hydrocarbons. Although condensed-phase hydrocarbons have a large amount of low-frequency modes that can efficiently dissipate the energy transferred to the surface in hyperthermal collisions with Ar atoms, the sizable cross section of prompt CID described in this paper and recent experiments indicate that degradation of condensed-phase hydrocarbons by 11-eV Ar atoms is probable.

Acknowledgment. This material is based upon work supported by the Air Force Office of Scientific Research (under Grant No. FA9550-06-1-0165) and by the National Science

Foundation (under Grant No. 0547543). The authors also wish to thank Timothy K. Minton (Montana State University) for providing unpublished experimental results.

References and Notes

(1) Bolton, K.; Hase, W. L. Direct dynamics simulations of reactive systems. In *Modern Methods for Multidimensional Dynamics Computations in Chemistry*; Thompson, D. L., Ed.; World Scientific: Singapore, 1998; pp 143.

(2) Bredow, T.; Jug, K. *Theor. Chem. Acc.* **2005**, *113*, 1.

(3) Gonzalez-Lafont, A.; Truong, T. N.; Truhlar, D. G. *J. Phys. Chem.* **1991**, *95*, 4618.

(4) Li, G.; Bosio, S. B. M.; Hase, W. L. *J. Mol. Struct.* **2000**, *556*, 43.

(5) Yan, T.-Y.; Doubleday, C.; Hase, W. L. *J. Phys. Chem. A* **2004**, *108*, 9863.

(6) Troya, D.; Garcia-Molina, E. *J. Phys. Chem. A* **2005**, *109*, 3015.

(7) Troya, D. *J. Chem. Phys.* **2006**, *123*, 214305/1.

(8) Troya, D.; Weiss, P. J. E. *J. Chem. Phys.* **2006**, *124*, 074313/1.

(9) Minton, T. K.; Garton, D. J. Dynamics of Atomic-Oxygen-Induced Polymer Degradation in Low Earth Orbit. In *Chemical Dynamics in Extreme Environments*; Dressler, R. A., Ed.; Advances Series in Physical Chemistry, Vol. 11; World Scientific: Singapore, 2001; pp 420.

(10) Murr, L. E.; Kinard, W. H. *Am. Sci.* **1993**, *82*, 505.

(11) Leger, L. J.; Visentine, J. T. *J. Spacecr. Rockets* **1986**, *23*, 505.

(12) Garton, D. J.; Minton, T. K.; Troya, D.; Pascual, R.; Schatz, G. C. *J. Phys. Chem. A* **2003**, *107*, 4583.

(13) Troya, D.; Pascual, R. Z.; Schatz, G. C. *J. Phys. Chem. A* **2003**, *107*, 10497.

(14) Troya, D.; Pascual, R. Z.; Garton, D. J.; Minton, T. K.; Schatz, G. C. *J. Phys. Chem. A* **2003**, *107*, 7161.

(15) Troya, D.; Schatz, G. C. *J. Chem. Phys.* **2004**, *120*, 7696.

(16) Troya, D.; Schatz, G. C. *Int. Rev. Phys. Chem.* **2004**, *23*, 341.

(17) Troya, D.; Schatz, G. C.; Garton, D. J.; Brunsvold, A. L.; Minton, T. K. *J. Chem. Phys.* **2004**, *120*, 731.

(18) Minton, T. K.; Zhang, J.; Garton, D. J.; Seale, J. W. *High Perform. Polym.* **2000**, *12*, 27.

(19) Brunsvold, A. L.; Garton, D. J.; Minton, T. K.; Troya, D.; Schatz, G. C. *J. Chem. Phys.* **2004**, *121*, 11702.

(20) Brunsvold, A. L.; Upadhyaya, H. P.; Zhang, J.; Minton, T. K. In *Proceedings of the 10th International Symposium on Materials in a Space Environment*, European Space Agency SP-616, 2006; Paper No. s4.1.minto/1.

(21) Troya, D. *J. Phys. Chem. A* **2005**, *109*, 5814.

(22) Alexander, W. A.; Troya, D. *J. Phys. Chem. A* **2006**, *110*, 10834.

(23) Frisch, M. J.; Trucks, G. W.; Schlegel, H. B.; Scuseria, G. E.; Robb, M. A.; Cheeseman, J. R.; Montgomery, J. J. A.; Vreven, T.; Kudin, K. N.; Burant, J. C.; Millam, J. M.; Iyengar, S. S.; Tomasi, J.; Barone, V.; Mennucci, B.; Cossi, M.; Scalmani, G.; Rega, N.; Petersson, G. A.; Nakatsuji, H.; Hada, M.; Ehara, M.; Toyota, K.; Fukuda, R.; Hasegawa, J.; Ishida, M.; Nakajima, T.; Honda, Y.; Kitao, O.; Nakai, H.; Klene, M.; Li, X.; Knox, J. E.; Hratchian, H. P.; Cross, J. B.; Bakken, V.; Adamo, C.; Jaramillo, J.; Gomperts, R.; Stratmann, R. E.; Yazyev, O.; Austin, A. J.; Cammi, R.; Pomelli, C.; Ochterski, J. W.; Ayala, P. Y.; Morokuma, K.; Voth, G. A.; Salvador, P.; Dannenberg, J. J.; Zakrzewski, V. G.; Dapprich, S.; Daniels, A. D.; Strain, M. C.; Farkas, O.; Malick, D. K.; Rabuck, A. D.; Raghavachari, K.; Foresman, J. B.; Ortiz, J. V.; Cui, Q.; Baboul, A. G.; Clifford, S.; Cioslowski, J.; Stefanov, B. B.; Liu, G.; Liashenko, A.; Piskorz, P.; Komaromi, I.; Martin, R. L.; Fox, D. J.; Keith, T.; Al-Laham, M. A.; Peng, C. Y.; Nanayakkara, A.; Challacombe, M.; Gill, P. M. W.; Johnson, B.; Chen, W.; Wong, M. W.; Gonzalez, C.; Pople, J. A. *Gaussian 03*, Revision C.02; Gaussian Inc.: Wallingford, CT, 2004.

(24) East, A. L. L.; Allen, W. D. *J. Chem. Phys.* **1993**, *99*, 4638.

(25) Halkier, A.; Helgaker, T.; Jorgensen, P.; Klopper, W.; Koch, H.; Olsen, J.; Wilson, A. K. *Chem. Phys. Lett.* **1998**, *286*, 243.

(26) Peterson, K. A.; Woon, D. E.; Dunning Jr., T. H. *J. Chem. Phys.* **1994**, 7410.

(27) Experimental reaction energy determined from the heats of formation at 298 K reported in the *NIST Chemistry WebBook*, available via the Internet at http://webbook.nist.gov/chemistry/.

(28) Experimental reaction energy determined from the heats of formation at 298 K reported in the *Chemical Kinetics and Photochemical Data for Use in Atmospheric Studies*, Evaluation Number 15, JPL Publication 06-2, available via the Internet at http://jpldataeval.jpl.nasa.gov/pdf/JPL_15_AllInOne.pdf.

(29) Experimental reaction energy determined from the heats of formation at 298 K listed on the Internet at http://www.iupac-kinetic.ch.cam.ac.uk/Thermo2003.pdf.

(30) Experimental reaction energy determined from the heats of formation at 0 K reported in the *Computational Chemistry Comparison and Benchmark Database*, available via the Internet at http://srdata.nist.gov/cccbdb/.

(31) Stewart, J. J. P. *J. Comput. Chem.* **1989**, *10*, 209.

(32) Dewar, M. J. S.; Zoebisch, E. G.; Healy, E. F.; Stewart, J. J. P. *J. Am. Chem. Soc.* **1985**, *107*, 3902.

(33) Ahlswede, B.; Jug, K. *J. Comput. Chem.* **1999**, *20*, 563.

(34) Dutta, A.; Sherrill, C. D. *J. Chem. Phys.* **2003**, *118*, 1610.

(35) Schmidt, M. W.; Baldridge, K. K.; Boatz, J. A.; Elbert, S. T.; Gordon, M. S.; Jensen, J. H.; Koseki, S.; Matsunaga, N.; Nguyen, K. A.; Su, S.; Windus, T. L.; Dupuis, M.; Montgomery, J. A. *J. Comput. Chem.* **1993**, *20*, 1347.

(36) Lenzer, T.; Luther, K.; Troe, J.; Gilbert, R. G.; Lim, K. F. *J. Chem. Phys.* **1995**, *103*, 626.